The Height Structure of the Solar Atmosphere from the EUV Perspective

J. Zhang, S. M. White, M. R. Kundu
Dept. of Astronomy, University of Maryland, College Park, MD 20742

ABSTRACT

We investigate the structure of the solar chromosphere and transition region using full Sun images obtained with the Extreme Ultraviolet Imaging Telescope (EIT) aboard the Solar and Heliospheric Observatory (SOHO) spacecraft. The limb seen in the EIT coronal images (taken in lines of Fe IX/X at 171 Å, Fe XII at 195 Å and Fe XV at 284 Å) is an absorption limb predicted by models to occur at the top of the chromosphere where the density of neutral hydrogen becomes significant ($\sim 10^{10}$ cm^{-3}). The transition-region limb seen in He II 304 Å images is an emission limb. We find: (1) the limb is higher at the poles than at the equator both in the coronal images (by 1300 $\pm$ 650 km) and the 304 Å images (by 3500 $\pm$ 1200 km); and (2) the 304 Å limb is significantly higher than the limb in the coronal images. The height difference is 3100 $\pm$ 1200 km at the equator, and 6600 $\pm$ 1200 km at the poles. We suggest that the elevation of the 304 Å limb above the limb in the coronal images may be due to the upper surface of the chromosphere being bumpy, possibly because of the presence of spicules. The polar extension is consistent with a reduced heat input to the chromosphere in the polar coronal holes compared with the quiet–Sun atmosphere at the equator.

Subject headings: Sun: chromosphere – Sun: transition region – Sun: UV radiation

1. Introduction

The height structure of the solar atmosphere is an important feature of any model of the atmosphere and its energy balance. The models for the lower atmosphere are largely based on the hydrostatic assumption and the idea of energy balance between energy loss, in the form of an outgoing radiation flux, and energy input, possibly in the form of non-thermal energy generated by turbulent sub-photospheric motions for the chromosphere and heat conduction from the hot corona for the transition region. The density and temperature gradients in the models are adjusted so that the predicted radiation in various spectral ranges matches the observations (e.g., Vernazza, Avrett & Loeser 1981, Fontenla, Avrett & Loeser 1993, Gu, Jefferies & Avrett 1997). The actual height structure in the chromosphere and transition region is difficult to resolve observationally, with the chromosphere being only of order $3''$ thick in these models and the transition region as little as $0\overset{''}{.}2$ thick. Both may be obscured at the limb by spicules and by magnetic loops projecting into the corona.

The observational evidence that does exist for the height structure is largely inconsistent with the models. Most models put the top of the chromosphere at heights ranging from 1700 to 2300 km above the photosphere (e.g., Anderson & Athay 1989, Fontenla, Avrett & Loeser 1993), whereas most observations in visible light during eclipses place it at about 5000 km (Zirin 1996). Radio observations during eclipses may also be used to determine the height of the chromosphere since short radio wavelengths become optically thick in the chromosphere: these have given heights of 3400 km at $\lambda = 0.85$ mm (Ewell, Jr. et al. 1993), 6000 km at 1.3 mm (Horne et al. 1981), 5500 km (Belkora et al. 1992) and 8000 km (White & Kundu 1994) at 3 mm. Recently Johannesson and Zirin (1996) measured the height of the chromosphere based on disk images of high-pass Hα filtergrams, and found that the chromospheric height varies with heliographic latitude, being 4400 km at the equator but about 6000 km at the poles. Usually, the large observed extension (5000 km) has been ignored on the grounds that it could be attributed to the numerous spicules which clearly show up in off-band Hα images. However, Zirin (1996) has argued that the height is indeed 5000 km and that most of the theoretical models are likely to be wrong because they are based on the possibly incorrect assumption of hydrostatic equilibrium.

In this paper, we present measurements of the height of chromospheric features as well as of the transition region using full Sun images obtained with the Extreme Ultraviolet Imaging Telescope (EIT; Delaboudinière et al. 1995, Moses et al. 1997) on the Solar and Heliospherical Observatory (SOHO) spacecraft. Although the resolution of these images ($2\overset{''}{.}6$ pixels) might not seem to lend itself to such a study, the radius of the limb present in EIT images can repeatably be measured with subpixel precision, and the height of the limb proves to be significantly above the photosphere. The advantages of EIT observations for this purpose are twofold: (1) full disk images provide us a chance to fit the entire limb of the lower solar atmosphere. (2) EIT images are sensitive to transition region and coronal temperatures, rather than chromospheric temperatures as in most other studies of the height of the limb. We find, in stark contrast to the solar photosphere which is highly circular (e.g., Kuhn et al. 1998), that the heights of the polar and equatorial limbs are very different in both the coronal and the transition region EIT images. (While revising this paper we became aware of a similar result obtained by Auchère et al. 1998 using a different technique.) The sense of this latitude dependence is in agreement with the optical result of Johanneson & Zirin (1996). In section 2 we discuss the nature of the limbs in the EIT images. In section 3, we present measurements and the results. The final section discusses the implications of the results.

2. The Solar Limb at EUV Wavelengths

EIT obtains images in four wavelength ranges centered on lines of the coronal species Fe IX/X (171 Å), Fe XII (195 Å), and Fe XV (284 Å), whose temperatures of maximum fractional abundance are about 1.0, 1.4 and 2.1 million K, respectively, and the transition–region diagnostic He II (304 Å), whose temperature of maximum fractional abundance is about 80,000 K. Inspection of EIT images indicates that the "limb" present in the images made in the coronal lines is an absorbing or occulting limb, whereas the limb in the 304 Å image is an emission limb. This is to be expected, since the 304 Å image should be dominated by transition region gas which is expected to be confined to a thin layer just above the chromosphere: thus 304 Å should show a sharp fall–off in intensity above the chromosphere which produces a well–defined emission limb. The coronal lines, however, are optically thin and arise in a range of heights throughout the corona: the limb in the coronal images appears where the lower atmosphere ceases to be optically thick to EUV radiation and the intensity jumps by a factor of 2 as emission from gas beyond the limb is added to that from gas in front of the limb.

Ionization of neutral H and He is the dominant absorption process for EUV photons (e.g., Cruddace et al. 1974). At 200 Å the cross–section for absorption is of order 2 $\times\ 10^{-19}$ cm^2 per neutral H atom (Rumph, Bowyer & Vennes 1994). In an exponential spherically symmetric atmosphere the line–of–sight column is $n_{H0}\,\sqrt{2\pi\,h_0\,R_\odot}$, where n_{H0} is the density of neutral hydrogen at the lowest point in the solar atmosphere along the line of sight and h_0 ($\ll R_\odot$) is the scale height of neutral hydrogen there. With a scale height of $h_0\ \sim 100$ km, which is plausible for the chromosphere, a neutral hydrogen density of only 10^{10} cm^3 is required to make the atmosphere opaque. This number is relatively insensitive to the actual scale height because of the square–root dependence on h_0. In both standard hydrostatic–equilibrium "VAL" atmospheric models (e.g., Vernazza, Avrett & Loeser 1981, Fontenla, Avrett & Loeser 1993) and empirically–determined models (e.g., Ewell, Jr. et al. 1993, Zirin 1996) such a density of neutral H is reached very close to the top of the chromosphere, which implies that the absorption limb seen in the EIT 171, 195 and 284 Å images should be the top of the chromosphere. The actual height in relation to the photosphere differs greatly between the two models: it is 1500 – 2000 km in the VAL models but 4700 km in Zirin's model. Note that the absorption cross–section at 284 Å is larger at about 4×10^{-19} cm^2, but given the small scale heights at the top of the chromosphere this is not sufficiently different that we expect to be able to measure a limb height at 284 Å which differs from the 171 and 195 Å heights.

3. Measurements and Results

We analyze data sets composed of full–disk, full–resolution EIT synoptic images in each of the four bandpasses acquired within a short time range (about 20 minutes) which have been taken several times daily since December 1996. That the images are taken nearly simultaneously minimizes the measurement uncertainties due to variations in the instrument and solar features. The measurements in this paper are based on 12 randomly–selected data sets evenly distributed between April 1997 and January 1998.

The size of the limb is determined by fitting the limb to an ellipse. Fitting is carried out by manually selecting limb points, typically 40 per image (examples are shown in Figure 1). Automated fitting routines do not generally work with high accuracy on EIT images due to the irregularity of the limb: we found the manual method to be tedious but reliable. The limb in these images is quite sharp: the brightness jumps from the disk value to the off–limb value within about three pixels along the radial direction. Thus, it is not difficult to select good limb points manually. We avoided emission enhancements above the limb due to features such as loop or arcade structures in coronal images and prominences and macro-spicules in the 304 Å images. The coordinates of individual limb points are only accurate to within one pixel, but the fitting procedure can determine the best–fit limb with sub–pixel accuracy. By using test subjects other than the authors, we verified that this method was repeatable and consistent. To improve statistical significance, the fit was carried out three times for each image. We determined the significance of ellipse fits by comparing them with circle fits: e.g., on 1997 Aug 03 the standard deviation of the distance of the selected points from the best-fit ellipse at 304 Å was 0.56 pixels, whereas for a circle it was 0.93 pixels. The difference was less significant at coronal wavelengths: an average of

0.43 pixels for the ellipse fit and 0.48 pixels for the circle fit.

As expected, the fits to the absorption limb in the three coronal images were generally consistent with one another: e.g., on 1997 Aug 03 the radius of the limb at the equator was 365.7, 365.8, and 365.7 pixels in the 171 Å, 195 Å and 284 Å images, respectively, while in the polar direction the radius was 366.3, 366.4 and 366.6 pixels, respectively. The radius of the limb in the coronal images is generally larger at the poles than at the equator by a small amount: e.g., 0.70 pixels larger on 1997 Aug. 03.

The emission limb in the 304 Å image is always found to be larger than the limb in the coronal images, e.g. on 1997 Aug. 03 the limb at 304 Å was 367.8 pixels at the equator and 369.8 pixels at the poles, which is 2.1 and 3.4 pixels larger than the corresponding limbs in the coronal images. In Figure 1 we compare the limbs in the 304 Å and 195 Å images directly for 1997 Aug. 03. The limbs at the poles and the east and west limbs are shown for both wavelengths, together with the line which represents the best fit to the 195 Å equatorial limb. The fact that the 195 Å limb is well inside the 304 Å transition-region-limb is clearly evident, as is the fact that the polar limbs at 304 Å are higher than the equatorial limbs. The difference between the polar and equatorial limbs in the coronal images is less than a pixel and is not readily apparent in Fig. 1.

In order to determine the significance of these pixel differences, we must first determine whether there is any asymmetry in the size of CCD pixels between the X (CCD rows) and Y (CCD columns) directions. For this purpose we analyzed a set of images taken on September 3, 1997, when the SOHO spacecraft was rotated 90° from its usual orientation. (SOHO operations generally maintain an alignment accuracy of better than 1° between the CCD Y axis and nominal solar rotation axis.) A synoptic set of EIT observations were taken at about 07:00 UT in nominal orientation (CCD Y-direction parallel to the solar rotation axis), and another at 13:00 UT after the 90° rotation (CCD Y-direction perpendicular to the solar rotation axis). We fitted the limb size in both data sets. In the coronal images the average limb radii at the equator and poles, respectively, were 367.7 $\pm$ 0.4 and 368.4 $\pm$ 0.4 pixels before rotation and 367.8 $\pm$ 0.4 and 368.3 $\pm$ 0.4 pixels after rotation. The 304 Å limb radii at the equator and poles, respectively, were 369.3 $\pm$ 0.8 and 372.6 $\pm$ 0.8 pixels before rotation and 369.3 $\pm$ 0.7 and 372.2 $\pm$ 0.7 pixels after rotation. These data clearly indicate that to within our measurement accuracy the pixels have identical X and Y dimensions on the sky, and that therefore the apparent differences between the polar and equatorial dimensions cannot be attributed to the pixel scale. Thus, the latitude dependence of the limb heights must be real.

We repeated the procedure described above for image sets on 11 other days almost evenly distributed over 7 months from April 1997 to January 1998. The relative height difference between the polar and equatorial limbs in the coronal images as a function of time is shown in Figure 2. It is significant and positive in all data sets, ranging from 800 km to 1790 km with an average of 1300 km (with a measurement uncertainty of 650 km). The height of the limb in the 304 Å images above the height of the limb in the coronal images as a function of time is also shown in Figure 2. The range of height at the poles is from about 5900 km up to 8100 km, while that at the equator is from about 2100 km to 4100 km. Both are consistent with being constant in time to within the measurement uncertainty (1200 km). The average height is 6600 $\pm$ 1200 km at pole and 3100 $\pm$ 1200 km at equator. The average difference between the polar and equatorial heights in the 304 Å images is 3500 $\pm$ 1200 km.

The size of the coronal limb in pixels scales very well with the distance of the SOHO spacecraft from the Sun, which varies by 3% over the period shown as SOHO orbits the Lagrangian L1 point between the Earth and the Sun. Averaged over the 12 measurements, we find that one EIT pixel is $2''\!.610 \pm 0''\!.002$ in both dimensions if the absorption limb in the coronal images is the photosphere (6.96×10^5 km). Note that the statistical uncertainty in this measurement is smaller than 0.1%, indicating that the feature responsible for the coronal limb is very stable over the 7 months. If the absorption is in the chromosphere at a height of 2000 km, the pixel scale would be $2''\!.617$.

4. Discussion and Conclusion

We have fit the solar limb in sets of EIT 171, 195, 284 and 304 Å synoptic images and find that (i) the three coronal lines images, where the limb is seen in absorption, yield an identical elliptic disk (to within our uncertainty) with the polar limb being 1300 km larger than the equatorial limb on average (ii) the 304 Å images, in which the transition-region limb is seen as an emission feature, invariably show a disk larger than in the coronal images, and also larger at the poles than at the equator. By detailed inspection of limb profiles of individual cases, we have determined that the radius we measure for the 304 Å limb corresponds to a point on the upper part of the decrease in intensity at the limb, whereas in the coronal images the radius we measure corresponds to a point near the base of the limb–brightening feature, i.e., just above the point where the intensity starts to increase sharply with radius at the limb. A careful inspection of average profiles at the limbs indicates that the peak in, e.g., the 195 Å images occurs at a slightly greater height than the peak in the 304 Å images, but that the rise towards the peak in the 195 Å images occurs well below the start of the fall–off in the 304 Å images. However, the average limb profiles are clearly not consistent with both the 304 Å and 195 Å images having a sharp edge at about the same height: there must exist 304 Å–emitting material above the coronal boundary. Note that the 304 Å limb determination is not affected by the contribution of coronal lines in the 304 Å bandpass: the relative contribution of the coronal lines can easily be determined by comparison with coronal images well above the limb, and is not significant at the limb.

A polar extension of the chromosphere would be consistent with a reduced heat input to the coronal hole atmosphere compared with the quiet Sun. Hydrostatic models for the solar atmosphere predict a more extended chromosphere when the energy supplied to the chromosphere is reduced, e.g. the height of VAL model A (dark point within a cell) is 250 km larger than that of VAL model F (very bright network element) and 500 km larger than that of VAL model P (plage area with medium brightness). The model of Basri et al (1979) predicts that the height of the chromosphere in a dark point is 1000 km larger than that of average quiet Sun. This occurs because the atmosphere must relax to a state in which the energy loss matches the energy input: since radiative energy loss varies as n^2, a more extended chromosphere produces smaller n for the same mass column and therefore reduces radiative losses. In this sense a larger chromospheric height at the poles would be consistent with the expected small heat input from the polar coronal holes

The 304 Å emission must arise in a region where the ambient He is singly ionized, which corresponds to a temperature of order 80000 K. If we assume that the transition region is truly as thin as all models predict and is a uniform sphere, then the solar limb in the 304 Å images should represent the top of the chromosphere. However, earlier we showed that the limb in coronal images should also be found at the top of the chromosphere where significant amounts of neutral H are present to absorb the EUV lines. The difference in height between the 304 Å limb and the limbs in the three coronal images is clearly not consistent with a model in which the chromosphere is a well–defined layer of uniform thickness and the 304 Å emission arises in a thin spherical surface at its upper edge.

The fact that the coronal limb lies *well below* the He II 304 Å limb requires either that (i) there be material at coronal temperatures extending to heights below the top of the surface on which 304 Å emission is to be found, or that (ii) all the coronal material lies radially above the 304 Å limb but the layer in the chromosphere which is opaque in the EUV and thus defines the coronal limb lies well below the 304 Å emitting layer, permitting a transparent window below the 304 Å limb through which coronal material beyond and in front of the limb may be seen.

The first of these two explanations suggests the plausible model of a bumpy interface between the corona and the chromosphere: effectively the height of the top of the chromosphere varies from place to place by up to several thousand kilometers, with the 304

Å emitting layer forming a skin (the transition region) on the upper surface of the bumpy chromosphere. The limb at 304 Å will then appear to be at the upper envelope of this surface, since 304 Å is in emission, while the coronal limb will be at the bottom envelope of the bumpy surface as long as the chromospheric fingers which protrude above the lower envelope do not produce significant absorption of the EUV radiation. The neutral hydrogen density in these “fingers” is likely to be lower than in the bulk of the chromosphere since they are surrounding by coronal material emitting ionizing radiation. The larger difference in height between the 304 Å limb and the coronal limb at the poles then implies that the top of the chromosphere is much “bumpier” at the poles than at the equator. The “bumpiness” of the top of the chromosphere could well be associated with spicules.

The second explanation requires that the level of ionization of H in the upper chromosphere be much higher than found in any current models of the chromosphere, since only if the density of neutral H and He is low can the upper chromosphere below the 304 Å emitting layer be transparent to EUV radiation at 171 – 284 Å. We note that He^+ can be ruled out as the main absorber since its absorption edge occurs at 228 Å and thus 284 Å photons are not absorbed by He^+.

One important unanswered question is whether the extension of the chromosphere at the pole is a local characteristic associated with only coronal holes, or a global feature which is associated with the poles but not directly with the presence of coronal holes there. The EIT images do not seem to be suitable to address this question: we would like to look for an extension of the 304 Å limb over a coronal hole at the equator, but locally it is a much harder task to identify and fit the limb than it is in the global sense which we have used here. Johannesson and Zirin (1996) in their H_α observations found that the polar height excess is co-spatial with the polar coronal holes, and that a similar excess is also found within active regions outside the polar region, although this may be unrelated.

5. ACKNOWLEDGMENTS

This research was supported by NASA grant NAG-5-6257 and NSF grant ATM-96-12738. We thank Markus Aschwanden and Alexander Nindos for their help in testing the fitting routine, and Ken Dere, Markus Aschwanden, Jeff Newmark, Bill Thompson and James A. Klimchuck for valuable discussions.

REFERENCES

Anderson, L. S., & Athay, R. G. 1989, ApJ, 336, 1089.

Auchère, F., Delaboudinière, J. P., Koutschmy, S., & Boulade, S. 1998, in Solar Jets and Coronal Plumes, ed. T.-D. Guyenne (Noordwijk: ESA SP 421), P. 245

Basri, G., Linsky, J. L., Bartoe, J.-D. F., Brueckner, G., & van Hoosier, M. E. 1979, ApJ, 230, 924.

Belkora, L., Hurford, G. J., Gary, D. E., & Woody, D. P. 1992, ApJ, 400, 692.

Cruddace, R., Paresce, F., Bowyer, S., & Lampton, M. 1974, ApJ, 187, 497.

Delaboudinière, J.-P., et al. 1995, Solar Phys., 162, 291.

Ewell, Jr., M. W., Zirin, H., Jensen, J. B., & Bastian, T. S. 1993, ApJ, 403, 426.

Fontenla, J. M., Avrett, E. H., & Loeser, R. 1993, ApJ, 406, 319.

Gu, Y., Jefferies, J. T., & Avrett, E. H. 1997, ApJ, 484, 960.

Horne, K., Hurford, G. J., Zirin, H., & de Graauw, T. 1981, ApJ, 244, 340.

Johannesson, A., & Zirin, H. 1996, ApJ, 471, 510.

Kuhn, J. R., Bush, R. I., Scheick, X., & Scherrer, P. 1998, Nat., 392, 155.

Moses, D., et al. 1997, Solar Phys., 175, 571.

Rumph, T., Bowyer, S., & Vennes, S. 1994, AJ, 107, 2108.

Vernazza, J. E., Avrett, E. H., & Loeser, R. 1981, ApJS, 45, 635.

White, S. M., & Kundu, M. R. 1994, in Infrared Solar Physics (IAU Symposium 154), ed. J. T. J. D. M. Rabin & C. Lindsey (Dordrecht: Kluwer Academic Publishers), P.167

Zirin, H. 1996, Solar Phys., 169, 313.

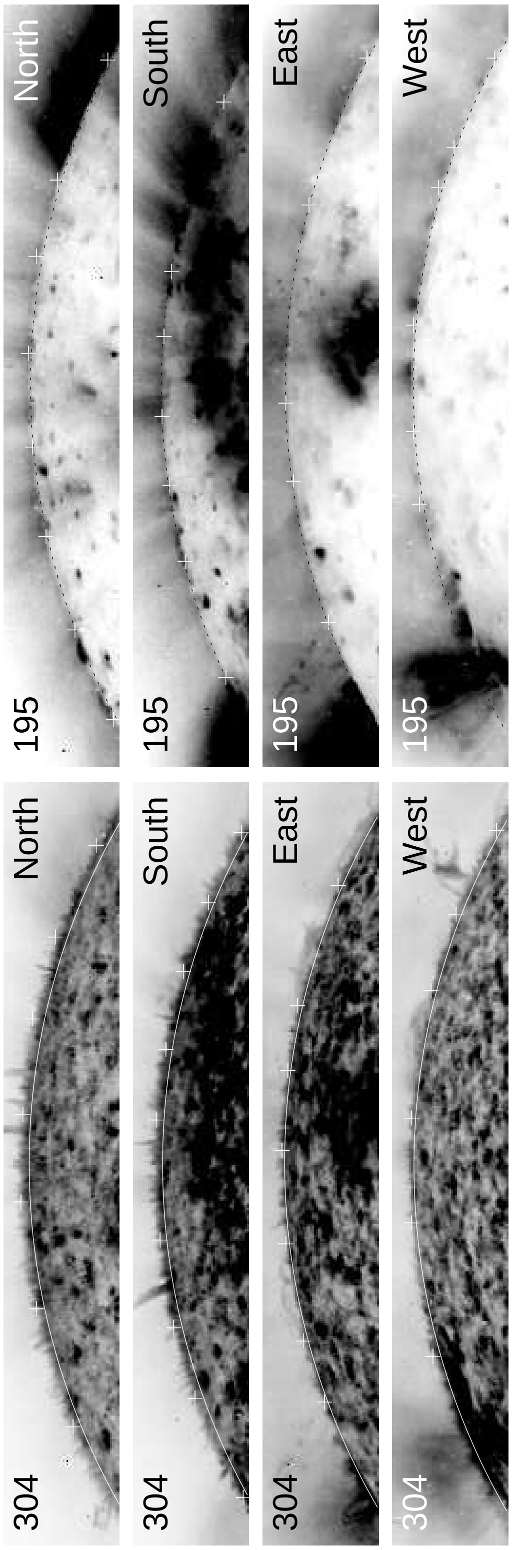

Fig. 1.— Comparison of the limb location in the EIT 304 Å (left panels) and 195 Å (right panels) on 1997 August 3. Each panel is a $1040'' \times 156''$ (400×60 pixels in the full–resolution images) region from either the north or south pole or the east or west limb, as marked. The relevant portion of the image has been rotated so that the limb is at the top of the image. In each panel, the equatorial limb from the fit of the 195 Å image has been plotted as a line (solid white line in the 304 Å panels, dotted black line in the 195 Å images), while pixels used in fitting the limbs are shown by crosses. Note that the fields of view in the corresponding 304 Å and 195 Å panels may differ by up to a pixel due to rounding.

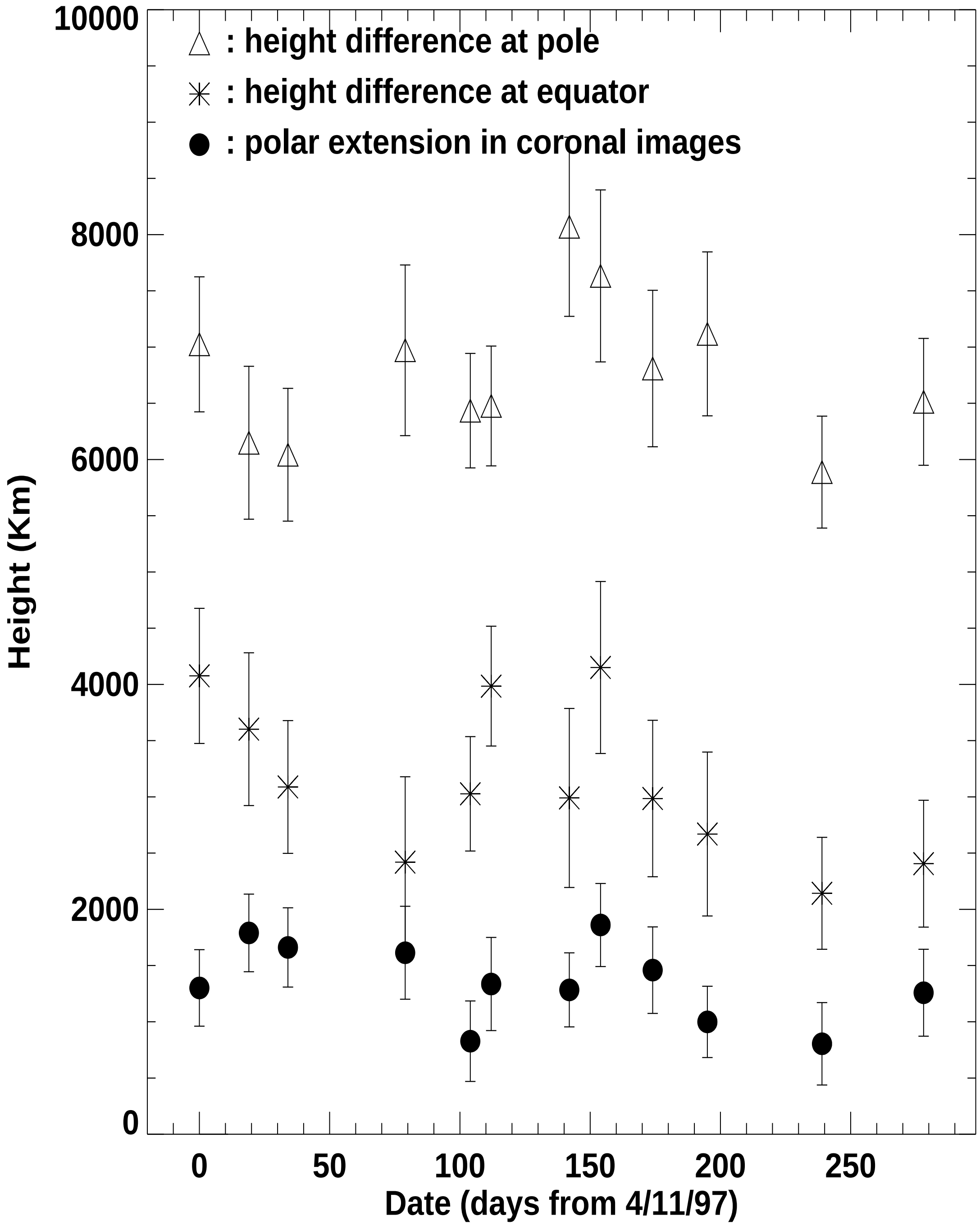

Fig. 2.— Heights of features in the EIT images: the height differences between the 304 Å limb and the limb in the coronal images at (i) the poles are marked by triangles, while the differences at (ii) the equator are marked by stars. (iii) The height of the polar limb above the equatorial limb in the coronal images is marked by filled circles. Measurements are plotted for each of the 12 data sets investigated. Error bars are plotted at $\pm\ \sigma$, where σ is the uncertainty in the fit of the limb points to an ellipse.